ELSEVIER

Chemical Engineering Science 63 (2008) 12–23

Chemical Engineering Science

www.elsevier.com/locate/ces

Heat and mass transfer of single droplet/wet particle drying

M. Mezhericher, A. Levy*, I. Borde

Pearlstone Centre for Aeronautical Engineering Studies, Department of Mechanical Engineering, Ben-Gurion University of the Negev, P.O. Box 653, Beer-Sheva 84105, Israel

Received 22 March 2007; received in revised form 10 August 2007; accepted 16 August 2007
Available online 24 August 2007

Abstract

A theoretical model, which considers the fully unsteady character of both heat and mass transfer during the drying of single droplet/wet particle, is presented. The model enables prediction of pressure and fraction distributions of air–vapour mixture within the capillary pores of the wet particle crust. The simulations of the drying process of a single silica droplet under different conditions show a permanent rising of pressure within the capillary pores, but the corresponding vapour fraction remains less than unity. The comparison between the drying histories of the silica droplet, predicted by the present model with the data, calculated by the model which assumes a quasi-steady-state mass transfer and linear pressure profile within the capillary pores, shows inconsiderable differences between the droplet/wet particle temperature and mass time-changes. At the same time, the present model predicts pressure build-up and temperature rising within the particle wet core. However, in the studied cases the temperature of the wet core temperature does not exceed the liquid saturation temperature and therefore no boiling of liquid within the particle wet core is observed.

Keywords: Drying; Heat transfer; Mass transfer; Particle; Crust; Mathematical modelling

1. Introduction

The study of heat and mass transfer of a single droplet, containing solids, is one of the important tasks for proper modelling of the spray drying process. Typically, the drying kinetics of a single droplet, containing solids, can be divided into two stages according to the morphology (see Fig. 1). Thus, in the first drying stage, the droplet with initial diameter ($d_{d,0}$ at Fig. 1) has greatest amount of liquid when it enters the drying medium. In the drying medium the droplet gains sensible heat (path 0–1 at Fig. 1) and then evaporation of liquid begins from the droplet surface. The process of liquid evaporation results in shrinkage of the droplet diameter (path 1–2 at Fig. 1). When the amount of liquid within the droplet falls to some critical value, a very thin layer of a dry solid crust is formed at the outer surface of the droplet (point 2 at Fig. 1). From this point the second drying stage begins (path 2–3 at Fig. 1) and the droplet is treated onwards as a wet particle with constant outer diameter (d_p at Fig. 1). The wet particle includes two separated regions: solid crust, which has a porous structure, and wet core, which consists of liquid and solids. During the second drying stage, as the result of simultaneous heat transfer to the wet particle and mass transfer to the drying agent, the thickness of the solid crust continuously increases, while the diameter of the wet core (d_i at Fig. 1) shrinks. The drying stops when the amount of liquid within the particle reduces to desired value.

Recently, we have critically reviewed the published theoretical drying models for both types of single droplets, containing either insoluble or dissolved solids (see Mezhericher et al., 2007a for details). The literature survey exposed various shortcomings of published models, such as steady-state conditions for heat and mass transfer equations, ignoring initial heating-up period of droplet, unjustified neglecting wet particle temperature profile, disregarding porosity of solid crust, inaccurate calculation of mass transfer rate. Also, some of the models were neglecting crust heat absorption and simplified droplet thermophysical properties were utilized. There was a lack of validation in a lot of cases as well. In addition, most of the published models were suitable to describe the drying

* Corresponding author. Tel.: +972 8 6477092; fax: +972 8 6477130.
E-mail address: avi@bgu.ac.il (A. Levy).

0009-2509/$ - see front matter © 2007 Elsevier Ltd. All rights reserved.
doi:10.1016/j.ces.2007.08.052

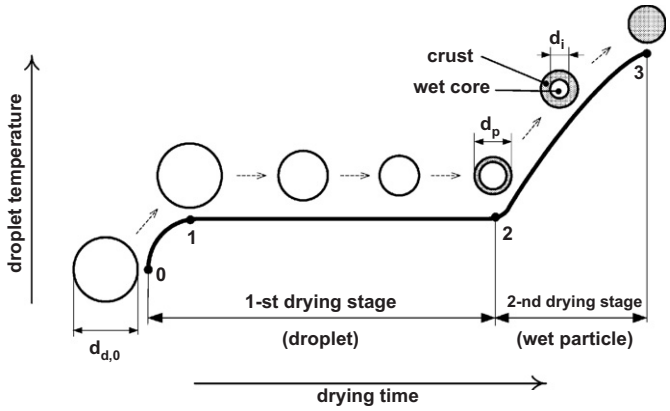

Fig. 1. Typical temperature curve and morphological changes during drying of single droplet containing solids.

of single droplet containing either insoluble or solely dissolved solids. Unlike the models found in the literature survey, the model of single droplet drying in atmospheric air, which took into account a fully time-dependent character of the heat transfer during the drying process and temperature profile within the droplet/wet particle, has been developed in the discussed paper (Mezhericher et al., 2007a). In this study, partial differential equations (PDEs) of heat transfer and ordinary differential equations (ODE) of mass transfer have been developed for the first and second drying stages. The period of droplet initial heating-up period, the heat capacity of the crust region, crust porosity and the temperature dependence of droplet/wet particle physical properties were also taken into account. In the second drying stage, it was assumed that the liquid evaporates from the wet core as the result of heat transfer from the drying air, and then the vapour moves through the pores of the crust towards the particle outer surface. This vapour movement inside the pores was assumed to be due to Stefan-type diffusion. From the particle outer surface the vapour was considered to be taken away by the mass convection mechanism. The corresponding mass transfer rate of the vapour was determined with the help of the steady-state equation proposed by Abuaf and Staub (1986). The set of theoretical equations was numerically solved and the model was successfully validated by comparing the predicted data with corresponding experimental results, available in the literature for silica and skim milk single droplets under different drying conditions.

The subject of our subsequent study (see Mezhericher et al., 2007b) was to investigate the reasons of possible cracking/rupture of a wet particle under elevated temperatures of the drying agent. It was supposed that dehumidification of the wet particle by the atmospheric air with temperature much greater than 100 °C can result in bubble formation and boiling inside the wet core of the particle (Nešić, 1990; Nešić and Vodnik, 1991). This process was considered to be responsible for the pressure rising under the porous crust. Consequently, if the difference between the pressure under the crust and the ambient pressure was greater than the crust tensile strength, it would lead to either cracking or rupture of the wet particle. Furthermore, if the discussed pressure difference exists, the mass transfer rate through the crust pores is the sum of corresponding diffusion and forced flow rates. However, the equation of Abuaf and Staub (1986), which we utilized previously for calculation of the vapour mass transfer rate (Mezhericher et al., 2007a), fails under such conditions. Thus, in the discussed paper (Mezhericher et al., 2007b) a modified equation was developed for evaluation of the vapour diffusion mass transfer rate; this equation took into account the time and the radius dependences of the pressure in the pores of the particle crust. The vapour forced mass transfer rate throughout the porous crust was determined with the help of Darcy's law equation (Cunningham and Williams, 1980). By assuming that the pressure changed linearly in the crust pores and supposing that the vapour mass transfer rate did not change along the pore, the set of model equations was numerically solved and simulations of colloidal silica drying were performed. The calculations showed that the temperatures of the particle wet core did not exceed the saturation value (i.e., no evidence for boiling). In addition, pressure rising within the particle core was not observed for a wide range of drying conditions. This behaviour was explained by the large porosity of the silica particles ($\varepsilon = 0.4$). Nevertheless, the elevated temperatures of drying air resulted in steep temperature differences between the wet particle outer surface and the wet core, which led to appearance of thermal stresses in the crust of the dried particle. The calculations of the thermal stresses and their comparisons to the crust failure criteria demonstrated, that the thermal stresses can be a reason of wet particle cracking/rupture and it depended on diameter of the dried particle, temperature of drying air and equivalent diameter of solids, which contain the initial droplet, at condition that all other drying parameters were fixed. In addition, it was observed that the tangential thermal stresses in the wet particle crust were predominant over the radial components (approx. 4.5 times more for silica particles).

As it can be seen, in our previous studies (Mezhericher et al., 2007a, b) the fully unsteady character of the heat transfer in both drying stages was considered, but the vapour mass transfer rate in the second drying stage was calculated by utilizing the quasi-steady-state conditions. Thus, in one study (see Mezhericher et al., 2007a), the vapour mass transfer rate was assumed to be due to Stefan-type diffusion only, and Abuaf and Staub's quasi-steady equation (Abuaf and Staub, 1986) was applied. In the subsequent paper (see Mezhericher et al., 2007b), the sum of vapour forced and Stefan-type diffusion mass transfer rates was determined by modifying the equation of Abuaf and Staub. This modified equation was solved by assuming a linear distribution of the pressure in the crust pores. It should also be noted that, in the model (Mezhericher et al., 2007b), it was assumed that the pressure over the particle wet core remained unchanged and equalled to the ambient pressure, when the temperature of the wet core was lower than the vapour saturation temperature at the ambient pressure. Otherwise, it was supposed that the wet core pressure was equal to the vapour saturation pressure at the wet core temperature.

The simplifications made in our previous models by coupling the unsteady-state PDE of heat transfer with quasi-steady-state

equations of mass transfer in the second drying stage, saved computer time need for drying simulations on the one hand. However, on the other hand these simplifications did not allow us to evaluate the profiles of vapour fraction and the pressure of air–vapour mixture within the particle crust. It should be noted that these distributions are difficult to measure experimentally, but they provide a lot of information about the character of the mass transfer process. The other important parameters, that also cannot be directly measured nowadays and may be predicted with the help of the drying kinetics model, are the temperature at the inner surface of the particle crust and the values of pressure and vapour fraction along the pores of particle crust. The analysis of these characteristics provides a deeper understanding of physical processes which occur within the wet particle during drying, e.g., mechanisms of mass transfer and pressure change within the capillary pores.

In the light of the above discussion, there is a need to develop a more realistic model for single droplet/wet particle drying, which takes into account the fully unsteady character of the heat and mass transfer in the second drying stage.

2. Objectives

The objective of the present study is to develop a theoretical drying model of single droplet/wet particle, which will consider the fully unsteady character of the heat and mass transfer in the second drying stage, and to perform the drying simulations that will allow us to study the mechanisms of mass transfer and pressure build-up within the wet particle.

3. Model description

3.1. First drying stage

In the first drying stage, drying of a motionless single droplet, containing solids, surrounded by a flow of atmospheric air, is modelled (see Fig. 2).

The heat transfer in the first drying stage is considered in a general case, namely that both conditions $Bi_d < 0.1$ and $Fo_d \geqslant 0.1$ are not satisfied simultaneously. Therefore, the droplet heat capacity cannot be considered as a lumped one and a temperature profile within the droplet should be taken into account. Assuming that the droplet is a sphere with isotropic properties and the coordinate origin is at the centre of the sphere, the equation of energy conservation in spherical coordinates can be written as (Mezhericher et al., 2007a)

$$\rho_d c_{p,d} \frac{\partial T_d}{\partial t} = \frac{1}{r^2} \frac{\partial}{\partial r} \left(k_d r^2 \frac{\partial T_d}{\partial r} \right), \quad 0 \leqslant r \leqslant R_d(t). \tag{1}$$

The corresponding boundary conditions are

$$\begin{cases} \dfrac{\partial T_d}{\partial r} = 0, \quad r = 0, \\ h(T_g - T_d) = k_d \dfrac{\partial T_d}{\partial r} + h_{fg} \dfrac{\dot{m}_v}{A_d}, \quad r = R_d(t). \end{cases} \tag{2}$$

The heat transfer from the drying air to the droplet occurs due to both convection and radiation phenomena. Therefore,

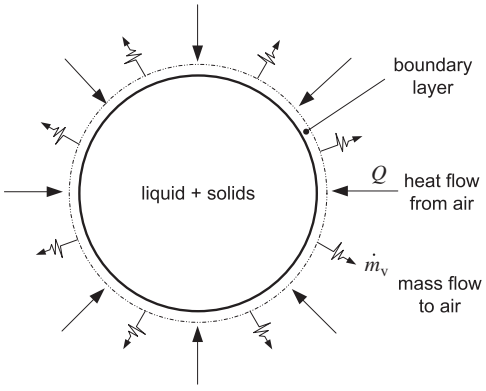

Fig. 2. Scheme of droplet dehumidification in the first drying stage.

the corresponding coefficient of heat transfer h can be evaluated as follows:

$$h = h_c + h_r. \tag{3}$$

The coefficient of convection heat transfer h_c is determined by the Nusselt number with the help of modified Ranz–Marshall correlations (Levi-Hevroni et al., 1995):

$$Nu_d = \frac{d_d h_c}{k_d} = (2 + 0.6 Re_d^{1/2} Pr^{1/3})(1 + B)^{-0.7}, \tag{4}$$

where $B = c_{p,v}(T_g - T_d)/h_{fg}$ is the Spalding number. The coefficient of radiation heat transfer can be found as (Holman, 2002)

$$h_r = \sigma \varepsilon_r (T_g^4 - T_d^4)/(T_g - T_d). \tag{5}$$

In the first drying stage the droplet has an excess of liquid which forms an envelope over the droplet surface, so the drying is similar to evaporation of pure liquid droplet. For this reason, the emissivity of droplet surface can be expected to be equal to this of the liquid fraction of the droplet, i.e., $\varepsilon_r = \varepsilon_{r,w}$.

The rate of liquid evaporation from the droplet surface is determined as

$$\dot{m}_v = h_D(\rho_{v,s} - \rho_{v,\infty})A_d. \tag{6}$$

Here the value of mass transfer coefficient h_D is evaluated from the corresponding Sherwood number (Levi-Hevroni et al., 1995)

$$Sh_d = \frac{d_d h_D}{D_v} = (2 + 0.6 Re_d^{1/2} Sc^{1/3})(1 + B)^{-0.7}. \tag{7}$$

By assuming the elementary droplet mass decreasing is proportional to elementary droplet diameter shrinkage, the droplet shrinkage rate is found as follows (Levi-Hevroni et al., 1995):

$$\frac{\mathrm{d}(R_d)}{\mathrm{d}t} = -\frac{1}{\rho_{d,w} 4\pi R_d^2} \dot{m}_v. \tag{8}$$

For the droplet moisture content, X, which is defined as mass ratio of liquid and solid fractions within the droplet, the following relation can be found:

$$X = m_{d,w}/m_{d,s} = m_d(1 + X_{d,0})/m_{d,0} - 1. \tag{9}$$

The droplet specific heat can be evaluated according to Kirillin and Sheindlin (1956):

$$c_{p,d} = \left(\frac{\partial q_t}{\partial T}\right)_p + c_{p,w}(1-c) + c_{p,s}c. \tag{10}$$

In the present study we consider only the ideal mixtures and solutions, so heat of mixing equals zero, i.e., $q_t = 0$. The mass fraction of solids and the droplet moisture content are connected:

$$c = 1/(1+X). \tag{11}$$

The droplet density can be estimated by considering a droplet as an ideal two-component mixture:

$$\rho_d = (1+X)\rho_{d,s}\rho_{d,w}/(\rho_{d,w} + X\rho_{d,s}). \tag{12}$$

In order to evaluate the droplet thermal conductivity, either series (13) or parallel (14) conceptions are applied (Chen and Peng, 2005):

$$k_d = \delta k_w + (1-\delta)k_s, \tag{13}$$

$$1/k_d = \delta/k_w + (1-\delta)/k_s, \tag{14}$$

where the droplet void fraction, δ, is calculated according to following expression:

$$\delta = V_{d,w}/V_d = 1 - 6m_{d,s}/(\pi\rho_{d,s}d_d^3). \tag{15}$$

The droplet mass can be obtained if we integrate (5):

$$m_d = m_{d,0} - 8/6\pi\rho_{d,w}(R_{d,0}^3 - R_d^3). \tag{16}$$

For drying air at atmospheric pressure the vapour diffusion coefficient can be calculated as follows (Grigoriev and Zorin, 1988):

$$D_v = 3.564 \times 10^{-10}(T_{d,s} + T_g)^{1.75}. \tag{17}$$

From Eqs. (10) and (12)–(14) it follows that the droplet specific heat, density and thermal conductivity are all functions of temperature. Therefore, for the set of equations (1)–(17) a numerical solution is preferred.

3.2. Second drying stage

3.2.1. Heat transfer

The second drying stage begins from the moment when droplet moisture content falls to the critical value and the process of porous crust formation begins on the surface of the droplet. From now, the droplet turns into a wet particle consisting of a dry porous crust surrounding a wet core. The outer diameter of wet particle remains unchangeable, but at the same time the particle wet core shrinks due to evaporation from its surface, and as a result the crust thickness increases. In our previous study (Mezhericher et al., 2007a) such scheme of the wet particle drying has been classified as a problem with internal moving evaporating interface. This moving interface is called crust–wet core interface or, simply, the interface in the present paper. The scheme of wet particle drying in the second drying stage is illustrated by Fig. 3.

The crust region, whose thermal conductivity is taken as temperature-independent, is considered as a shell of a hollow sphere pierced by a large number of identical straight cylindrical capillaries. By assuming that the wet particle physical properties are isotropic and the coordinate origin is at the centre of the particle, two following equations of energy conservation with corresponding boundary conditions can be written in spherical coordinates:

Crust region of the dried particle:

$$\frac{\partial T_{cr}}{\partial t} = \frac{\alpha_{cr}}{r^2}\frac{\partial}{\partial r}\left(r^2\frac{\partial T_{cr}}{\partial r}\right), \quad R_i(t) \leqslant r \leqslant R_p, \tag{18}$$

$$\begin{cases} k_{cr}\dfrac{\partial T_{cr}}{\partial r} = k_{wc}\dfrac{\partial T_{wc}}{\partial r} + h_{fg}\dfrac{\dot{m}_v}{A_i}, & r = R_i(t), \\ T_{wc} = T_{cr}, & r = R_i(t), \\ h(T_g - T_{cr}) = k_{cr}\dfrac{\partial T_{cr}}{\partial r}, & r = R_p. \end{cases} \tag{19}$$

Wet core region of the dried particle:

$$\rho_{wc}c_{p,wc}\frac{\partial T_{wc}}{\partial t} = \frac{1}{r^2}\frac{\partial}{\partial r}\left(k_{wc}r^2\frac{\partial T_{wc}}{\partial r}\right), \quad 0 \leqslant r \leqslant R_i(t), \tag{20}$$

$$\begin{cases} \dfrac{\partial T_{wc}}{\partial r} = 0, & r = 0, \\ k_{cr}\dfrac{\partial T_{cr}}{\partial r} = k_{wc}\dfrac{\partial T_{wc}}{\partial r} + h_{fg}\dfrac{\dot{m}_v}{A_i}, & r = R_i(t), \\ T_{cr} = T_{wc}, & r = R_i(t). \end{cases} \tag{21}$$

The droplet temperature at the point of critical moisture content is an initial condition for both Eqs. (18) and (20).

In the second drying stage the coefficient of heat transfer, h, is calculated in the same way as that described above for the first drying stage (see Eqs. (3)–(5)). The only difference is that the emissivity of the particle outer surface ε_r is assumed to be equal to the corresponding value of emissivity of the particle solid fraction, i.e., $\varepsilon_r = \varepsilon_{r,s}$.

The receding rate of crust–wet core interface is connected with the rate of liquid evaporation from this interface (Levi-Hevroni et al., 1995):

$$\frac{\mathrm{d}(R_i)}{\mathrm{d}t} = -\frac{1}{\varepsilon\rho_{wc,w}4\pi R_i^2}\dot{m}_v. \tag{22}$$

3.2.2. Mass transfer.

In order to describe the process of liquid evaporation from the crust–wet core interface inside the wet particle and subsequent vapour flow through the crust pores to the ambient, let us consider an isolated capillary pore of the particle crust. The scheme of capillary pore is illustrated by Fig. 4.

In the present model the capillary pore is treated as a straight cylindric body. Therefore, it is convenient to apply the mass, the momentum and the energy conservation laws for the control volume (capillary pore) in cylindrical coordinate system. The origin of this system is at the crust–wet core interface and axis z coincides with the line of pore symmetry (see Fig. 4).

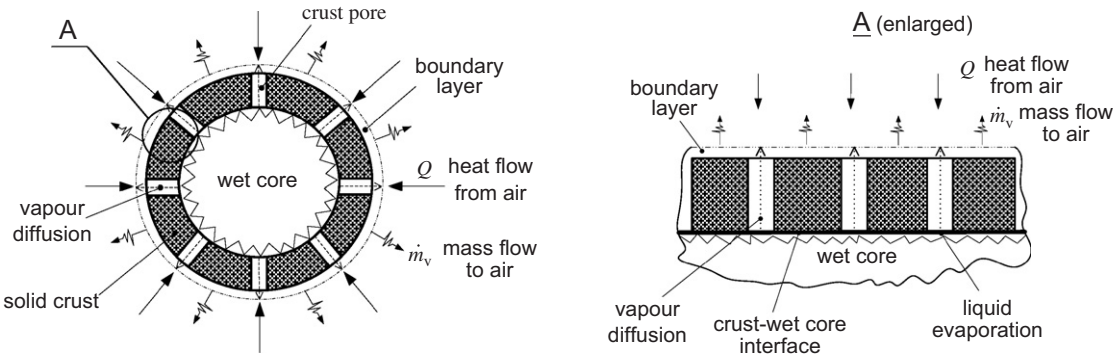

Fig. 3. Scheme of wet particle dehumidification in the second drying stage.

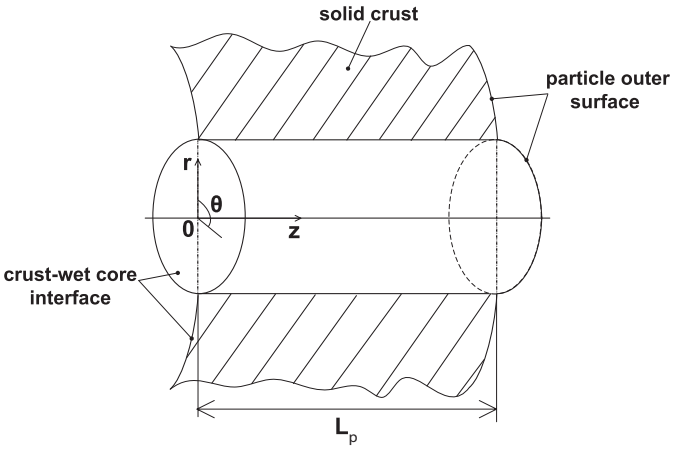

Fig. 4. Scheme of capillary pore within the crust of wet particle.

3.2.2.1. Mass conservation. Assuming that within the cylindric crust pore the air–vapour mixture flows isotropically along z-axis only, the equation of mass conservation can be written as follows (Burmeister, 1983):

$$\frac{\partial \rho}{\partial t} + \frac{\partial}{\partial z}(\rho v_z) = 0. \tag{23}$$

3.2.2.2. Momentum conservation. The development of momentum conservation equation brings us to three separate expressions (Burmeister, 1983):

r-component:

$$\frac{\partial p}{\partial r} = 0 \quad \Rightarrow \quad p \neq f(r). \tag{24}$$

θ-component:

$$\frac{\partial p}{\partial \theta} = 0 \quad \Rightarrow \quad p \neq f(\theta). \tag{25}$$

z-component:

$$\rho\left(\frac{\partial v_z}{\partial t} + v_z\frac{\partial v_z}{\partial z}\right) = -\frac{\partial p}{\partial z} + \frac{1}{r}\frac{\partial}{\partial r}(r\tau_{rz}) + \frac{1}{r}\frac{\partial \tau_{\theta z}}{\partial \theta} + \frac{\partial \tau_{zz}}{\partial \theta} + \rho g_z. \tag{26}$$

If we assume that only τ_{rz} component of shear stress is non-zero (see Cunningham and Williams, 1980 for details) and the gravity term is negligible, we obtain from Eq. (26):

$$\rho\left(\frac{\partial v_z}{\partial t} + v_z\frac{\partial v_z}{\partial z}\right) = -\frac{\partial p}{\partial z} + \frac{1}{r}\frac{\partial}{\partial r}(r\tau_{rz}). \tag{27}$$

The shear stress at rz-plane is calculated as (Burmeister, 1983)

$$\tau_{rz} = \mu\frac{\partial v_z}{\partial r}. \tag{28}$$

Substituting Eq. (28) into Eq. (27), we get

$$\rho\left(\frac{\partial v_z}{\partial t} + v_z\frac{\partial v_z}{\partial z}\right) = -\frac{\partial p}{\partial z} + \frac{\mu}{r}\frac{\partial}{\partial r}\left(r\frac{\partial v_z}{\partial r}\right). \tag{29}$$

Since the crust pore has a small radius, which is in order of microns, we can expect that the air–vapour flow within the pores will be laminar ($Re < 2100$). Therefore, the viscous forces (right-hand side of Eq. (29)) are much greater than the inertial forces (left-hand side of Eq. (29)). Under such condition, the integration of Eq. (29) brings us to well-known Darcy's law for flow through the porous media (Cunningham and Williams, 1980):

$$v_z = -\frac{B_k}{\mu}\frac{A_{\text{total}}}{A_{\text{pores}}}\frac{\partial p}{\partial z} = -\frac{B_k}{\mu\varepsilon^{\beta}}\frac{\partial p}{\partial z}. \tag{30}$$

3.2.2.3. Mass diffusion. By determining the vapour fraction ω_v as

$$\omega_v = \rho_v/\rho, \tag{31}$$

and assuming that it changes solely along z-axis of the crust pore, the vapour movement through the crust pores can be described by the following equation of binary diffusion (Burmeister, 1983):

$$\rho\left(\frac{\partial \omega_v}{\partial t} + v_z\frac{\partial \omega_v}{\partial z}\right) = \frac{\partial}{\partial z}\left(\rho D_v\frac{\partial \omega_v}{\partial z}\right). \tag{32}$$

The coefficient of vapour diffusion in the air D_v is found from semi-empirical correlation (Eckert and Drake, 1972):

$$D_v = 2.302 \times 10^{-5}\frac{p_0}{p}\left(\frac{T}{T_0}\right)^{1.81}, \tag{33}$$

where $p_0 = 0.98 \times 10^5$ Pa and $T_0 = 256$ K.

3.2.2.4. Energy conservation. The generalized equation of energy conservation in cylindrical coordinates is (Burmeister, 1983)

$$\rho\frac{\mathrm{D}c_P T}{\mathrm{D}t}+\mathrm{div}(-k\nabla T)=\frac{\mathrm{D}p}{\mathrm{D}t}+q'''+\mu\Phi. \tag{34}$$

In the considered case, there is no heat source inside the pore, thus $q'''=0$. For gases typically $Pr\cdot Ec\ll 1$ and so the conduction term $\mathrm{div}(-k\nabla T)$ is much greater than viscous dissipation term $\mu\Phi$; therefore, the latter can be neglected in Eq. (34). In the present study we also suppose that due to small length of capillary pore, the changes of air–vapour mixture temperature along the pore are negligible. Consequently, the above temperature is equal to the temperature of the crust–wet core interface. Such an assumption allows us to consider only time dependence of the temperature inside the pores of the particle crust. In addition, the behaviour of air–vapour mixture is considered to be close to ideal gas.

As the result of above assumptions, the equation of energy conservation (34) can be reduced to the following:

$$\rho c_p\frac{\mathrm{d}T}{\mathrm{d}t}=\frac{\partial p}{\partial t}+v_z\frac{\partial p}{\partial z}. \tag{35}$$

3.2.2.5. Constitutive equation. The equation of state for the air–vapour mixture within the capillary pore (by assuming ideal gas) is

$$p=\frac{\rho}{M}\Re T. \tag{36}$$

The main interest of our current work is finding the values and distributions of the vapour fraction and pressure within the pores of particle crust. Therefore, the obtained set of five equations (23), (30), (32), (35) and (36) is transformed in order to obtain an explicit dependence of the pressure and vapour fraction on time and space coordinates. These transformations are described below.

The equation of mass conservation (23) can be rewritten as

$$\frac{\mathrm{d}\rho}{\mathrm{d}t}+\rho\frac{\partial v_z}{\partial z}=0. \tag{37}$$

Substituting the equation of state (36) into Eq. (37), yields:

$$M\frac{\mathrm{d}p}{\mathrm{d}t}+p\frac{\mathrm{d}M}{\mathrm{d}t}-\frac{pM}{T}\frac{\mathrm{d}T}{\mathrm{d}t}+pM\frac{\partial v_z}{\partial z}=0. \tag{38}$$

Performing the same operation on Eq. (35), we get

$$\frac{\mathrm{d}T}{\mathrm{d}t}=\frac{\Re T}{Mc_p p}\left(\frac{\partial p}{\partial t}+v_z\frac{\partial p}{\partial z}\right) \tag{39}$$

or

$$\frac{\mathrm{d}T}{\mathrm{d}t}=\frac{\Re T}{Mc_p p}\frac{\mathrm{d}p}{\mathrm{d}t}. \tag{40}$$

Differentiating Eq. (30) by z and neglecting permeability, viscosity and porosity changes along the pore, yields

$$\frac{\partial v_z}{\partial z}=-\frac{B_k}{\mu\varepsilon^\beta}\frac{\partial^2 p}{\partial z^2}. \tag{41}$$

Substituting Eqs. (40) and (41) into Eq. (38), we obtain

$$M\frac{\mathrm{d}p}{\mathrm{d}t}+p\frac{\mathrm{d}M}{\mathrm{d}t}-\frac{\Re}{c_p}\frac{\mathrm{d}p}{\mathrm{d}t}-\frac{B_k M}{\mu\varepsilon^\beta}p\frac{\partial^2 p}{\partial z^2}=0. \tag{42}$$

For air–vapour mixture it can be shown that

$$M=\frac{M_a M_v}{M_v(1-\omega_v)+\omega_v M_a}, \tag{43}$$

and therefore

$$\frac{\mathrm{d}M}{\mathrm{d}t}=-\frac{M_a M_v(M_a-M_v)}{[M_v(1-\omega_v)+\omega_v M_a]^2}\frac{\mathrm{d}\omega_v}{\mathrm{d}t}, \tag{44}$$

$$\frac{\mathrm{d}M}{\mathrm{d}t}=-\frac{M_a-M_v}{M_a M_v}M^2\frac{\mathrm{d}\omega_v}{\mathrm{d}t}. \tag{45}$$

Analogously,

$$\frac{\partial M}{\partial z}=-\frac{M_a-M_v}{M_a M_v}M^2\frac{\partial\omega_v}{\partial z}. \tag{46}$$

Substituting Eq. (45) into Eq. (42), we get finally:

$$\frac{1}{\gamma p}\frac{\mathrm{d}p}{\mathrm{d}t}=\frac{M_a-M_v}{M_a M_v}M\frac{\mathrm{d}\omega_v}{\mathrm{d}t}+\frac{B_k}{\mu\varepsilon^\beta}\frac{\partial^2 p}{\partial z^2}, \tag{47}$$

where $\gamma=c_p/c_v$ is specific heat ratio.

The above equation establishes dependence of both vapour fraction and pressure of air–vapour mixture on time and space coordinates. In order to solve this equation, another relation between p and ω_v, is needed. For this purpose, the equation of mass diffusion (32) is rewritten as follows:

$$\rho\frac{\mathrm{d}\omega_v}{\mathrm{d}t}=\frac{\partial}{\partial z}\left(\rho D_v\frac{\partial\omega_v}{\partial z}\right). \tag{48}$$

Then, by utilizing the equation of state (36), we get

$$pM\frac{\mathrm{d}\omega_v}{\mathrm{d}t}=\frac{\partial}{\partial z}\left(pM\,D_v\frac{\partial\omega_v}{\partial z}\right). \tag{49}$$

Subsequently, differentiation of Eq. (33) gives

$$\frac{\partial D_v}{\partial z}=2.302\times 10^{-5}\,p_0\left(\frac{T}{T_0}\right)^{1.81}\left(-\frac{1}{p^2}\right)\frac{\partial p}{\partial z}$$

or

$$\frac{\partial D_v}{\partial z}=-D_v\frac{1}{p}\frac{\partial p}{\partial z}. \tag{50}$$

Then, using Eqs. (46) and (50), Eq. (49) can be rewritten as follows:

$$\frac{\mathrm{d}\omega_v}{\mathrm{d}t}=D_v\left[\frac{\partial^2\omega_v}{\partial z^2}-\frac{M_a-M_v}{M_a M_v}M\left(\frac{\partial\omega_v}{\partial z}\right)^2\right]. \tag{51}$$

The above equation describes the second relation between p and ω_v.

The obtained set of two differential equations (47) and (51), which describe the distribution of pressure and vapour fraction within the pore of particle crust, is the subject for further numerical solution. For this reason, appropriate initial and boundary conditions are developed below.

Initial conditions: When a solid crust begins to form, the pressure of air–vapour mixture within an infinitesimal crust pore can be assumed equal to the ambient pressure. The corresponding vapour fraction is calculated as the ratio of partial vapour density to total density of air–vapour mixture over the droplet surface at the end of the first drying stage.

Boundary conditions: In the present study we consider that evaporation of the liquid from the crust–wet core interface is equivalent to inflow of the vapour mass into the pores of the particle crust. The corresponding rate of vapour mass inflow equals the rate of evaporation from the crust–wet core interface:

$$(\rho_v v_{z,v})_{\text{in}} A_{\text{pores}} = \dot{m}_v. \tag{52}$$

Here A_{pores} is the mean area of particle crust cross-section, occupied by pores (Mezhericher et al., 2007b):

$$A_{\text{pores}} = 4\pi\varepsilon^{\beta} R_p R_i. \tag{53}$$

The mass balance for the vapour fraction at the boundary $z = 0$:

$$(\rho_v v_{z,v})_{\text{in}} = -\rho D_v \frac{\partial \omega_v}{\partial z} + \omega_v(\rho v_z)\bigg|_{z=0} \quad \text{when } z = 0. \tag{54}$$

On the other hand, continuity requires

$$(\rho_v v_{z,v})_{\text{in}} = (\rho v_z)|_{z=0}. \tag{55}$$

Substituting Eq. (55) into Eq. (54), we get

$$-\rho D_v \frac{\partial \omega_v}{\partial z} = (1-\omega_v)(\rho v_z)_{z=0} \quad \text{when } z = 0. \tag{56}$$

By substituting Eq. (52), the above equation can be rewritten as

$$-\rho D_v \frac{\partial \omega_v}{\partial z} = (1-\omega_v)\frac{\dot{m}_v}{A_{\text{pores}}} \quad \text{when } z = 0. \tag{57}$$

Finally, substituting Eqs. (22) and (53) into Eq. (57), we obtain

$$\rho D_v \frac{\partial \omega_v}{\partial z} = (1-\omega_v)\varepsilon^{1-\beta}\rho_{wc,w}\frac{R_i}{R_p}\frac{\mathrm{d}(R_i)}{\mathrm{d}t} \quad \text{when } z = 0. \tag{58}$$

In the present study we assume that the liquid fraction in the particle wet core is in equilibrium with the vapour over the crust–wet core interface, i.e.,

$$\omega_v = \rho_{v,\text{sat}}(T_{wc,s})/\rho \quad \text{when } z = 0. \tag{59}$$

Then, the pressure of air–vapour mixture at the crust–wet core interface can be found by combining the above equation with the ideal gas law (36):

$$p = p_{v,\text{sat}}(T_{wc,s})\frac{M_v}{\omega_v M} \quad \text{when } z = 0. \tag{60}$$

For the second boundary of the capillary pore ($z = L_p$), the following equation of mass conservation for vapour fraction can be developed:

$$\left[-\rho D_v \frac{\partial \omega_v}{\partial z} + \omega_v(\rho v_z)\right] A_{\text{pores}} = \rho h_D(\omega_v - \omega_{v,\infty}) A_p \quad \text{when } z = L_p$$

or

$$-\rho D_v \frac{\partial \omega_v}{\partial z} + \omega_v(\rho v_z) = \rho h_D(\omega_v - \omega_{v,\infty})\frac{R_p}{R_i}\varepsilon^{-\beta} \quad \text{when } z = L_p. \tag{61}$$

In the present paper it is assumed that the pressure at the particle outer surface is equal to the drying air pressure. Therefore, for $z = L_p$:

$$p|_{z=L_p} = p_g. \tag{62}$$

Combining the above condition with the equation of state (36) and substituting the result into Eq. (61), yields to

$$-D_v \frac{\partial \omega_v}{\partial z} + \omega_v(\rho v_z)\frac{\Re T_{wc,s}}{p_g M} = h_D(\omega_v - \omega_{v,\infty})\frac{R_p}{R_i}\varepsilon^{-\beta} \quad \text{when } z = L_p. \tag{63}$$

In such a way, the pressure of air–vapour mixture and the vapour fraction within the capillary pores of the particle crust is determined by the set of differential equations (47) and (51), and their boundary conditions (58), (60), (62) and (63).

4. Numerical solution of the developed model

In the present study, an original numerical solution procedure has been developed and realized as a computer program. The procedure is based on the algorithm proposed by Moyano and Scarpettini (2000).

4.1. First drying stage

The PDE (1) is solved simultaneously with its boundary conditions (2) and additional equations (3)–(17). The numerical solution is complicated due to the presence of a variable spatial domain $0 \leqslant r \leqslant R_d(t)$. This difficulty is overcome by applying the fully implicit finite difference scheme with fixed time-step.

4.2. Second drying stage

In order to obtain the numerical solution of the developed model, the above mentioned fully implicit finite difference scheme with fixed time-step is applied for each of PDE (18) and (19), which represent the energy conservation in the regions of particle crust and wet core. Then, the set of non-linear PDE (47) and (51) and their boundary conditions (58), (60), (62) and (63), determining the distributions of pressure and vapour fraction within the capillary pore of the particle crust, have been discretized according to the procedure, given in the paper of Moyano and Scarpettini (2000). A predictor–corrector method for numerical solution of non-linear PDE is implemented (see Ames, 1965, for details). Finally, two sets of algebraic equations, which are obtained after above discretization of Eqs. (18), (19) and (47), (51), are coupled by utilizing common boundary conditions at the crust–wet core interface.

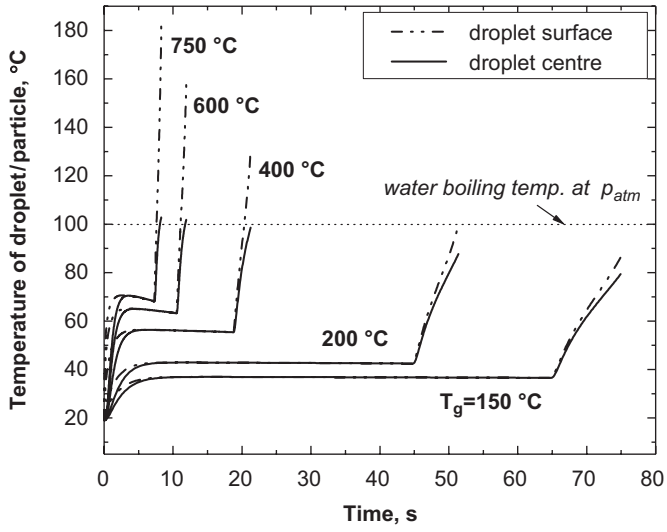

Fig. 5. Temperature history of silica droplet/wet particle.

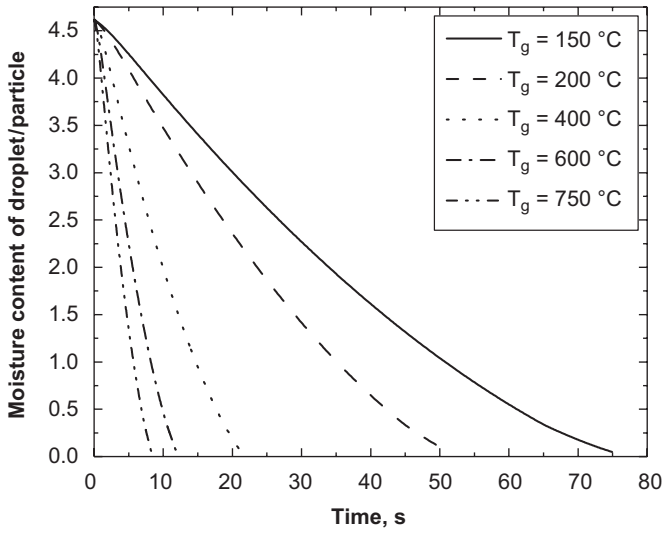

Fig. 7. Moisture content history of silica droplet/wet particle.

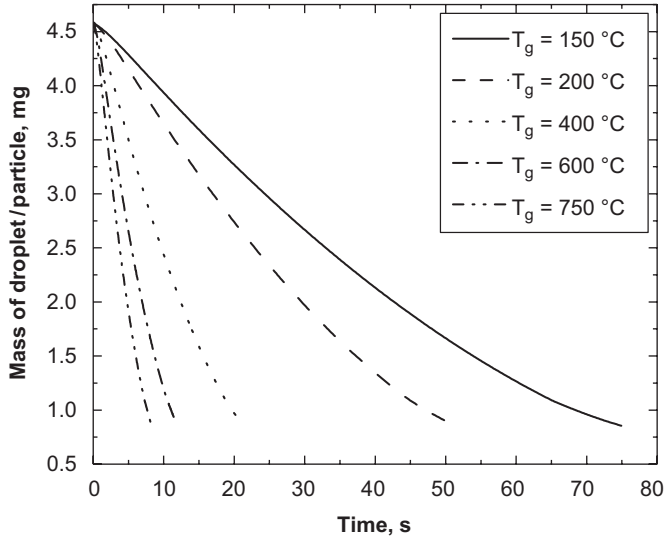

Fig. 6. Mass history of silica droplet/wet particle.

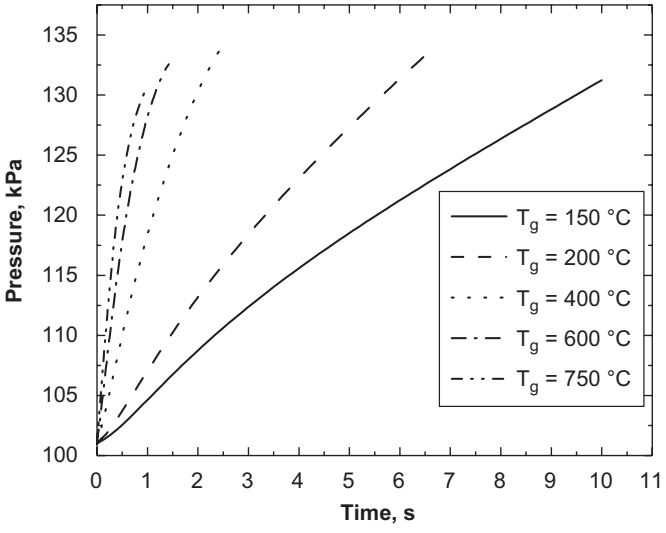

Fig. 8. Pressure over the crust–wet core interface in the second drying stage.

5. Results of calculations

With the help of numerical solution of the developed model, drying simulations of a droplet containing colloidal silica particles (primary particles) have been performed. The dried slurry consists of mono-dispersed amorphous silica spherical particles (median size of primary particle was 0.272 μm, density was 1950 kg/m^3), deflocculated in water with an initial volume fraction of primary particles of 0.10 (see Minoshima et al., 2002 for details). No specific binder is utilized. The emissivities of droplet liquid and solid fractions are considered as fixed values and are set $\varepsilon_{r,w} = 0.96$ and $\varepsilon_{r,s} = 0.8$ correspondingly (see Knudsen, 1997). During the studies, different parameters are varied: drying air temperature is changed in the range of 150–750 °C, drying air velocity is 0.25–3.5 m/s, initial droplet diameter is 0.25–2 mm and porosity of the particle crust is altered between 0.1 and 0.4. The important characteristics of the droplet/wet particle are tracked during the simulations: temperature of the droplet centre and outer surface, droplet mass and moisture content, vapour fraction and pressure of air–vapour mixture over the crust–wet core interface within the particle pores.

A number of calculation results predicted by the developed model for different temperatures of drying air are illustrated by Figs. 5–9. In these simulations we have utilized the following values of drying parameters: initial droplet temperature $T_{d,0} = 19$ °C; initial droplet diameter $d_{d,0} = 2$ mm; particle crust porosity $\varepsilon = 0.4$ and final moisture content $X_f = 0.05$. The velocity of the drying air has been set $u_g = 1.4$ m/s.

At the same drying conditions as mentioned above, Figs. 10 and 11 demonstrate typical distributions of vapour fraction and pressure of air–vapour mixture within the capillary pores at the end of the drying process ($X_f = 0.05$). The character of these distributions is common for the whole process in the second drying stage.

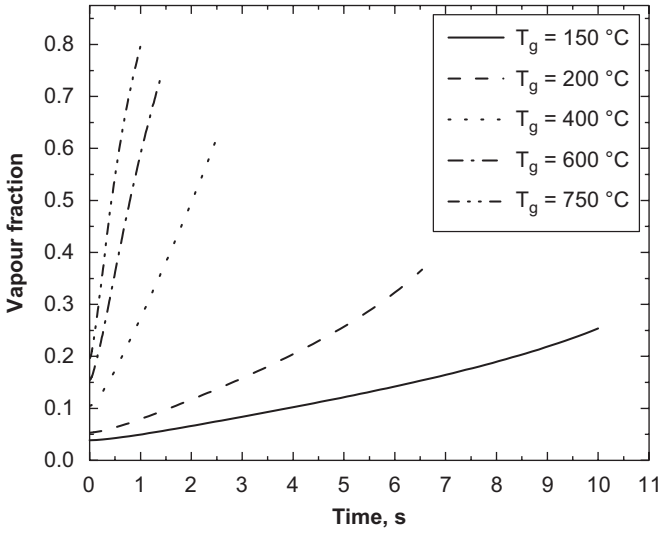

Fig. 9. Vapour fraction over the crust–wet core interface in the second drying stage.

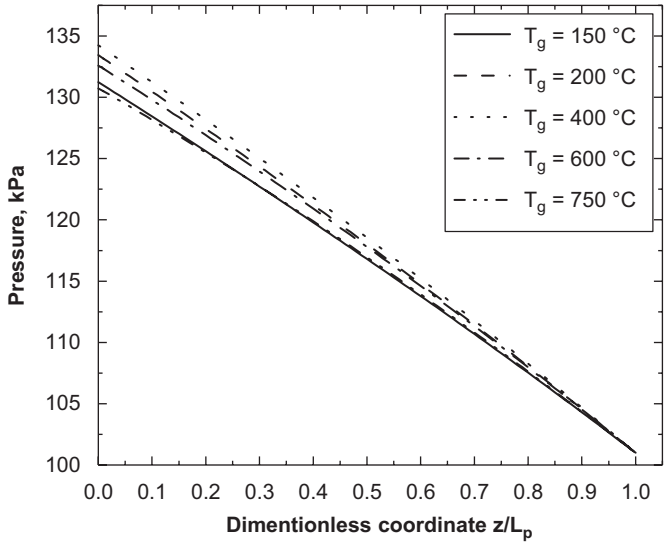

Fig. 11. Typical distribution of the pressure within the capillary pores at the end of drying process ($X_f = 0.05$).

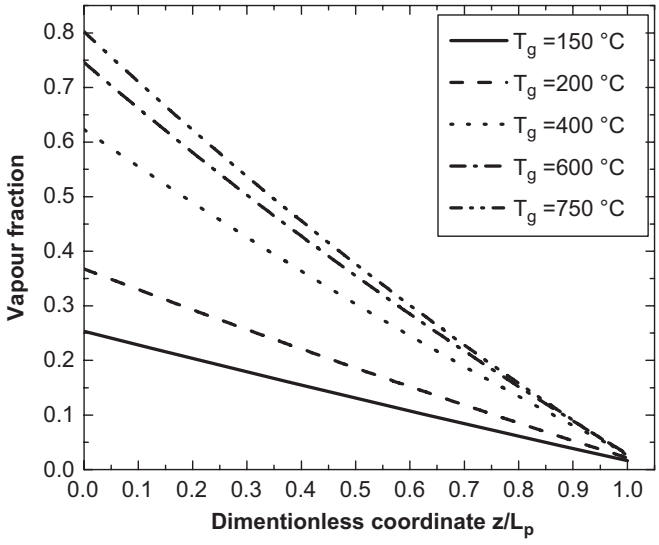

Fig. 10. Typical distribution of the vapour fraction within the capillary pore at the end of drying process ($X_f = 0.05$).

As mentioned above, the simulations with the help of the developed model have been performed using various drying conditions, such as different values of drying air temperatures and velocities, initial droplet diameters and particle crust porosities (the studied ranges of these parameters have been referred before). However, it has been found that the main drying characteristics demonstrate similar behaviour in all the investigated cases, so that in the current paper these characteristics are presented as functions of the drying air temperature only.

6. Discussion

The predicted history of silica droplet temperature under different drying conditions shows the existence of temperature difference between the particle outer surface and its centre (see Fig. 5). As can be seen, this difference is zero at the beginning of the second drying stage and grows permanently in course of drying, reaching a maximum value at the end of the drying process. On the other hand, the maximum temperature difference increases with higher temperatures of the drying air. Thus, the maximum temperature difference varies between $\sim 7\,^{\circ}\mathrm{C}$ for $T_g = 150\,^{\circ}\mathrm{C}$ and $\sim 80\,^{\circ}\mathrm{C}$ for $T_g = 750\,^{\circ}\mathrm{C}$.

It should be noted that at the drying air temperatures of 600 and 750 °C the temperature of the wet core exceeds 100 °C (the boiling temperature at atmospheric pressure).

The histories of droplet mass and droplet moisture content, which are shown in Figs. 6 and 7, demonstrate similarity during the drying process: maximum value at the beginning of the drying and then gradual decreasing in time.

Figs. 8 and 9 present the pressure and the vapour fraction over the crust–wet core interface during the second drying stage. From these figures there can be seen a gradual increase of pressure and vapour fraction over the interface between the crust and the wet core. This can be explained in the following way: rise of the particle temperature leads to evaporation of the liquid fraction in the particle wet core, and, as consequence, increases the vapour fraction and partial vapour pressure over the crust–wet core interface. On the other hand, the partial pressure of dry air over the above interface gradually reduces during drying as the result of dry air diffusion from the drying medium through the pores towards the particle wet core and the forced flow of air–vapour mixture in opposite direction. The imbalance of these two processes: increase of the pressure of vapour fraction and decrease of the pressure of dry air fraction, results in the build-up of air–vapour mixture pressure over the interface between the crust and wet core. The corresponding value of vapour fraction also rises. Consequently, it led us to the conclusion that in the studied cases the diffusion mechanism of vapour flow plays more important role than forced vapour

flow due to pressure difference inside the pores of the particle crust.

If we analyse the data presented in Figs. 8 and 9, it can be concluded that in spite of the fact that pressure difference between the wet core and the surrounding rises up to 30% of the pressure of the drying air, the corresponding values of vapour fraction remain less than unity ($\omega_v|_{z=0} < 1$) in all studied cases. Since the core temperature is lower than the saturation temperature at the core pressure, boiling does not occur (although, the core temperature rises above 100 °C, which is the saturation temperature of the particles surrounding).

Typical distributions of vapour fraction and pressure along the crust pores are presented in Figs. 10 and 11. As can be seen, both the vapour fraction and the pressure decrease linearly from the particle core towards it outer surface.

After analysing the behaviour of drying characteristics calculated with the help of the present model, it was decided to compare its predictions with our previous model (Mezhericher et al., 2007b). The first drying stage of both the present and the previous models is described by the same set of equations and therefore only calculation results in the second drying stage of the two models are considered. The main difference between the models is the way of modelling the mass transfer from the wet core to the drying air. The results of comparison for silica droplet drying under different temperatures of drying air are illustrated in Fig. 12. The following values of drying parameters have been applied in the simulations: $T_{d,0}=19\,°C$, $d_{d,0}=2\,mm$, $u_g = 1.4\,m/s$, $\varepsilon = 0.4$ and $X_f = 0.05$.

From Fig. 12a it can be seen that the curves of particle surface temperature, predicted by two different models, are nearly coinciding and the maximum discrepancy does not exceed 1.32%. The temperatures in the particle centre (see Fig. 12b), calculated by two different ways, show slight difference (about 1.2% maximum) for drying air temperatures of $T_g = 150$, 200 and 400 °C. It can be noted that for $T_g = 600$ and 750 °C, our previous model (Mezhericher et al., 2007b) predicts that corresponding temperatures of particle centre lie below 100 °C at the end of the drying process. From the present model it can be seen that these temperatures are above 100 °C. So, the greatest difference in temperatures of particle centre is 2.29% for $T_g = 600\,°C$ and it equals to 2.92% for $T_g = 750\,°C$. The particle mass time-change shows a very good agreement in all considered cases (see Fig. 12c), and the largest deviation between the curves corresponding to the different models is lower than 0.12%.

It should be noted that, in contrast to the present model, the calculations made using the model (Mezhericher et al., 2007b) did not demonstrate pressure increase over the crust–wet core interface during drying. The reason for this is that in the model (Mezhericher et al., 2007b) the increasing of pressure over the particle wet core was connected with the wet core temperature, and, therefore, particle cracking/rupture due mechanical stresses (which result from the pressure difference between the inner and outer surfaces of the particle crust) could not be predicted by the previous model (Mezhericher et al., 2007b).

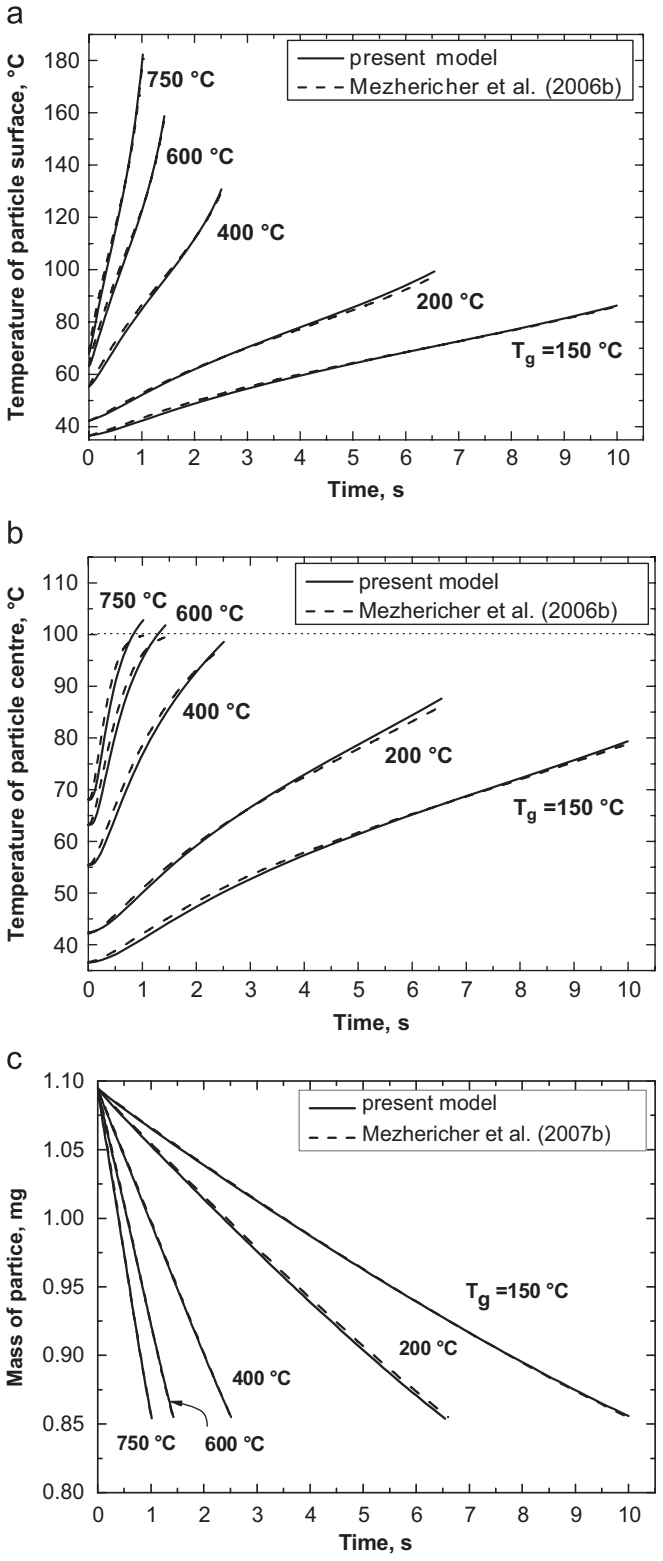

Fig. 12. Drying history of silica droplet in the second drying stage under different temperatures of drying air: (a) temperature of the particle outer surface; (b) temperature of the centre of the particle; (c) mass of the particle.

7. Conclusions

In the present study a theoretical model of heat and mass transfer of single droplet/wet particle drying has been

developed. Unlike our previously published models (Mezhericher et al., 2007a, b), the developed one considers the fully unsteady character of heat and mass transfer in the second drying stage and enables calculation of the pressure and vapour fraction of air–vapour mixture within the capillary pores of the particle crust. The model equations have been numerically solved and simulations of the drying process of single silica droplet have been performed. During the studies, the drying air temperature, drying air velocity, initial droplet diameter and porosity of the particle crust were varied in wide ranges. In order to reduce the length of the paper, only the influence of drying agent temperature was presented.

An important finding in the present study was the continuous rising of the pressure inside the particle over the crust–wet core interface. The model prediction was explained by imbalance of two concurrent processes. The first process results from liquid evaporation at the crust–wet core interface, which causes vapour mass flow inside the pores by diffusion and forced mechanisms. The second process is dry air movement within the pores: diffusion of the dry air from the surrounding towards the interface and dry air forced flow in opposite direction. In that way, it was concluded that in the studied cases the diffusion mechanism of vapour flow played a more important role than forced vapour flow due to pressure difference inside the pores of the particle crust.

The developed model showed that no boiling of the liquid inside the particle wet core was observed in the studies performed (see previous section).

The comparison between the drying histories of colloidal silica droplet predicted by the developed model with the data calculated utilizing our previous model (Mezhericher et al., 2007b), showed insignificant differences for both droplet temperature and mass time-changes under different drying conditions. In our previous model (Mezhericher et al., 2007b) we have described the process of mass transfer in the second drying stage by utilizing the assumptions of quasi-steady-state and linear pressure profile within the crust pores (as it can be seen, typical pressure distributions, presented in Fig. 11, confirmed the justification of the last assumption). As a result, the obtained mass transfer equations were much simpler than developed in the present study, which considers the full time dependence. Therefore, our previous model (Mezhericher et al., 2007b) requires less computer time for calculations and this fact gives us the opportunity to apply the above model with reasonable accuracy for cases when fast computations are necessary. On the other hand, if one needs to obtain more detailed information about wet particle behaviour during drying: the exact temperature, pressure and vapour fraction values at the crust–wet core interface and/or the pressure and vapour fraction distributions within the pores of the crust, the model developed in the present paper will be very helpful. This model can be also utilized for prediction of particle cracking/rupture during drying due to both temperature and mechanical stresses, which result from corresponding temperature and pressure differences between the inner and outer surfaces of the particle crust.

Notation

A	surface area, m^2
A_{pores}	mean area of crust cross-section, occupied by pores, m^2
A_{total}	total mean area of crust cross-section, m^2
b	empirical coefficient
B	Spalding number
Bi	Biot number
B_k	crust permeability, m^2
c	mass concentration of solid fraction, $kg\,kg^{-1}$
c_p	specific heat under constant pressure, $J\,kg^{-1}\,K^{-1}$
c_v	specific heat under constant volume, $J\,kg^{-1}\,K^{-1}$
d	diameter, m
D_v	coefficient of vapour diffusion, $m^2\,s^{-1}$
Ec	Eckert number
Fo	Fourier number
g	acceleration of gravity, $m\,s^{-2}$
h	heat transfer coefficient, $W\,m^{-2}\,K^{-1}$
h_c	coefficient of convection heat transfer, $Wm^{-2}\,K^{-1}$
h_D	mass transfer coefficient, $m\,s^{-1}$
h_{fg}	specific heat of evaporation, $J\,kg^{-1}$
h_r	coefficient of radiation heat transfer, $W\,m^{-2}\,K^{-1}$
k	thermal conductivity, $W\,m^{-1}\,K^{-1}$
L_p	length of crust pore, m
m	mass, kg
M	molecular weight, $kg\,mol^{-1}$
$\dot{m}_v$	rate of evaporation, $kg\,s^{-1}$
n	empirical coefficient
Nu	Nusselt number
p	pressure, Pa
p_0	reference pressure, Pa
Pr	Prandtl number
q_t	specific heat of mixing, $J\,kg^{-1}$
q''	heat source term, $W\,m^{-3}$
r	radial coordinate, m
R	radius, m
$\Re$	universal gas constant, $J\,mol^{-1}\,K^{-1}$
Re	Reynolds number
s	space coordinate, m
Sc	Schmidt number
Sh	Sherwood number
t	time, s
T	temperature, K
T_0	reference temperature, K
u_g	velocity of drying agent, $m\,s^{-1}$
V	volume, m^3
X	moisture content (dry basis), $kg\,kg^{-1}$
z	axial coordinate, m

Greek letters

α	thermal diffusivity, $m^2\,s^{-1}$
α_m	empirical coefficient
α_T	coefficient of thermal expansion, K^{-1}
β	empirical power coefficient

γ	specific heat ratio
δ	droplet void fraction
ε	crust porosity
ε_r	emissivity
θ	angular coordinate
μ	dynamic viscosity, $\mathrm{kg\,m^{-1}\,s^{-1}}$
ρ	density, $\mathrm{kg\,m^{-3}}$
σ	Stefan–Boltzmann constant, $\mathrm{W\,m^{-2}\,K^{-4}}$
τ	shear stress, Pa
υ	velocity, $\mathrm{m\,s^{-1}}$
Φ	dissipation term, $\mathrm{J\,kg^{-1}\,m^{-2}}$
ω_v	vapour fraction

Subscripts

a	air, dry air fraction
atm	atmospheric
c	crust capillary
cr	particle crust
d	droplet
f	final point of drying process
flow	forced flow
g	drying agent
i	crust–wet core interface
in	inflow
m	air–vapour mixture
out	outflow
p	particle
pores	crust pores
r	radial direction
s	solid fraction or surface
sat	saturated
v	vapour, vapour fraction
w	water
wc	particle wet core
z	axial direction
0	initial point of drying process
∞	bulk of drying agent
θ	tangential direction

Acknowledgement

We wish to thank the Israel Ministry of Immigrant Absorption for partial support of this work.

References

Abuaf, N., Staub, F.W., 1986. Drying of liquid–solid slurry droplets. In: Mujumdar, A.S. (Ed.), Drying '86, vol. 1. Hemisphere, Washington, DC, pp. 277–284.

Ames, W.F., 1965. Nonlinear Partial Differential Equations in Engineering. Academic Press, New York.

Burmeister, L.C., 1983. Convective Heat Transfer. Wiley, New York.

Chen, X.D., Peng, X.F., 2005. Modified Biot number in the context of air drying of small moist porous objects. Drying Technology 23, 83–103.

Cunningham, R.E., Williams, R.J.J., 1980. Diffusion in Gases and Porous Media. Plenum Press, New York.

Eckert, E.R.G., Drake, R.M., 1972. Heat and Mass Transfer. McGraw-Hill, New York.

Grigoriev, V.A., Zorin, V.M., 1988. Thermal Engineering Handbook. Part 1, Moscow (in Russian).

Holman, J.P., 2002. Heat Transfer. McGraw-Hill, New York.

Kirillin, V.A., Sheindlin, A.E., 1956. Thermodynamics of solutions, Moscow (in Russian).

Knudsen, J.G., et al., 1997. Heat and mass transfer. In: Perry, R.H., Green, D.W., Maloney, J.O. (Eds.), Perry's Chemical Engineers Handbook. McGraw-Hill, New York, pp. 1–5.

Levi-Hevroni, D., Levy, A., Borde, I., 1995. Mathematical modelling of drying of liquid/slurries in steady state one-dimensional flow. Drying Technology 13, 1187–1201.

Mezhericher, M., Levy, A., Borde, I., 2007a. Theoretical drying model of single droplets containing insoluble or dissolved solids. Drying Technology 25 (6), 1025–1032.

Mezhericher, M., Levy, A., Borde, I., 2007b. Modelling of particle breakage during drying. Chemical Engineering and Processing ⟨http://dx.doi.org/10.1016/j.cep.2007.06.018⟩.

Minoshima, H., Matsushima, K., Liang, H., Shinohara, K., 2002. Estimation of diameter of granule prepared by spray drying of slurry with fast and easy evaporation. Journal of Chemical Engineering of Japan 35, 880–885.

Moyano, E.A., Scarpettini, A.F., 2000. Numerical stability study and error estimation for two implicit schemes in a moving boundary problem. Numerical Methods for Partial Differential Equations 16, 42–61.

Nešić, S., 1990. The evaporation of single droplets—experiments and modelling. In: Mujumdar, A.S. (Ed.), Drying '89. Hemisphere, New York, pp. 386–393.

Nešić, S., Vodnik, J., 1991. Kinetics of droplet evaporation. Chemical Engineering Science 46, 527–537.